Non-contact Measurement of Line Voltage

David Lawrence, John Donnal, and Steven Leeb

***Abstract*—This paper presents a capacitively coupled non-contact voltage sensor which is specifically optimized for monitoring line voltage. The sensor uses two non-vibrating capacitive pickups to measure the rate of change of an unknown potential, and digitally integrates that rate of change in order to recover the original signal. This architecture allows for higher sensitivity and more robust disturbance rejection than previous designs have offered. The cost of the sensor is low because the number of parts is small and the capacitive pickups are integrated into a standard printed circuit board.**

I. Introduction

Non-contact measurement of electric potential has proven useful for circumstances in which it is difficult to establish Ohmic contact with the conductors in question. Non-contact sensors offer ease of installation and robust high-voltage isolation in exchange for lower accuracy and increased susceptibility to external disturbances.

Non-contact measurement of static electric potentials was first proposed by [1] in 1928. A vibrating plate is placed near an unknown potential, forming a time-varying capacitance. The voltage of the vibrating plate is adjusted until the vibrations induce no current through the plate, indicating that the plate's potential is equal to the unknown potential. The bandwidth of the sensor is limited by the vibration frequency of the plate. Reference [2] proposes a method by which the residual current through the sensor plate is integrated to determine the higher frequency components of the unknown potential.

Recent work has focused on capacitive sensors that do not vibrate. The induced current is integrated to obtain the unknown potential at all frequencies of interest. Reference [3] uses a capacitor to perform the integration. References [4] and [5] are optimized for the geometry of high voltage transmission lines. However, the gain of non-vibrating capacitive sensors is dependent upon the distance to the unknown conductor. Two sensor plates can be separately measured to compensate for this dependence [6]. Alternatively, large sensor plates can be placed close to a wire in order to enter a regime of operation in which the transfer function is not dependent on the separation distance [7].

The unique challenge of non-contact voltage sensing is *reconstructing the input signal while rejecting pickup from other sources*. Specifically, the currents induced by the input signal must be integrated in order to recover the input voltage. However, the currents induced by other sources have significant low-frequency components, which are amplified by an ideal integrator. There is a fundamental tradeoff between the accuracy of voltage measurements and a sensor's signal-to-noise ratio.

This paper describes a non-contact voltage sensor based on [8]. The new sensor takes a differential measurement of two vertically stacked non-vibrating sensor plates in order to *maximize* the dependence of gain on plate-to-wire distance, so that the signal from a nearby wire is selected and the signals from more distant wires are rejected. The sensor is especially well suited measurements that do not require the absolute scaling factor to be determined (e.g. total harmonic distortion and line regulation).

A new analog circuit integrates the capacitive pickups and amplification into a $2\,\mathrm{cm}^2$ printed circuit board requiring less than \$3 of discrete components. The resulting signal is processed by a new digital filter which provides superior disturbance rejection and an exceptionally accurate frequency response.

II. Principle of operation

A parasitic capacitance C_p develops between a sensor plate and a nearby wire. The sensor plate is attached to AC ground by a resistance R and a capacitance C. The transfer function from the wire voltage to the sensor plate voltage is given by

$$\frac{V_o(s)}{V_i(s)} = \frac{sRC_p}{sR(C+C_p)+1}. \tag{1}$$

Conventional capacitive-divider sensors choose R to be very large. The transfer function is then approximated by

$$\frac{V_o(s)}{V_i(s)} \approx \frac{C_p}{C+C_p}.$$

If C is kept much smaller than C_p (which requires careful construction), the equation simplifies further to $V_o(s) \approx V_i(s)$. Unfortunately, this approach is not

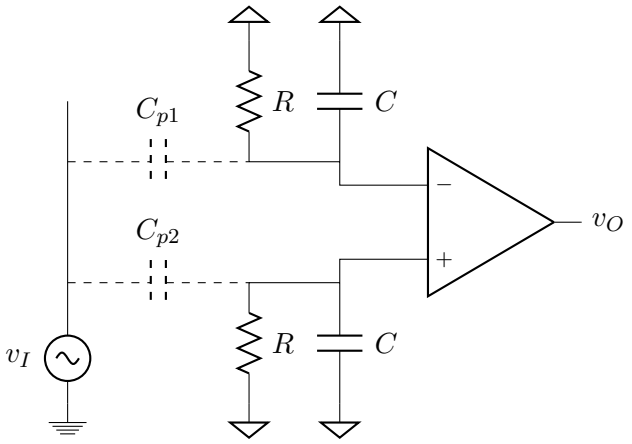

Fig. 1. Circuit for differential non-contact sensing of an AC voltage. Equation (3) provides the transfer function of this circuit.

practical for the new sensor because C_p is tiny and the resistance required would impractically large.[1]

Instead, the new sensor operates in the regime where

$$|sR(C + C_p)| \ll 1$$

and so

$$\frac{V_o(s)}{V_i(s)} \approx sRC_p. \tag{2}$$

The sensitivity of the sensor is proportional to frequency. It is inversely proportional to the distance d between the wire and the sensor plate, because

$$C_p \propto \frac{1}{d}.$$

Note that the sensor measures the input signal v_I relative to its own ground, which must be connected (or at least AC coupled) to the input signal's ground.

As proposed by [8], improved localization is obtained by taking a differential measurement from two stacked sensor plates. This arrangement is shown in Fig. 1. Parasitic capacitance between the two plates is neglected from this model because in the differential mode it is equivalent to additional capacitance between each plate and ground.

The exact transfer function of the differential sensor is given by

$$\frac{V_o(s)}{V_i(s)} = \frac{sR(C_{p2} - C_{p1})(sRC + 1)}{(sR(C + C_{p1}) + 1)(sR(C + C_{p2}) + 1)}. \tag{3}$$

[1]We are concerned with values of C_p as low as $0.1\,\mathrm{pF}$ and the lowest frequency of interest is $60\,\mathrm{Hz}$. To place the breakpoint of the RC network at one tenth of that frequency would require a $265\,\mathrm{G\Omega}$ resistor. Such impedances require the most exacting construction and cannot be achieved on a standard printed circuit board.

For frequencies satisfying $|sRC| \ll 1$, the transfer function is approximated by

$$\frac{V_o(s)}{V_i(s)} \approx sR(C_{p2} - C_{p1}) \tag{4}$$

which is analogous to (2) for the single-plate sensor.

If the sensor plates are at a distance d from the wire and separated from each other by a distance $d_0 \ll d$, the differential capacitance is

$$C_{p2} - C_{p1} \propto \frac{1}{d} - \frac{1}{d + d_0} \approx \frac{d_0}{d^2}.$$

Therefore the sensitivity of the differential sensor is inversely proportional to the *square* of the distance between the wire and the sensor plates.

An alternative approximation aids in understanding the frequency-dependent behavior of the differential sensor. When $C_{p1} \ll C$ and $C_{p2} \ll C$, the transfer function is roughly

$$\frac{V_o(s)}{V_i(s)} \approx \frac{sR(C_{p2} - C_{p1})}{sRC + 1}. \tag{5}$$

The input voltage is recovered by integrating the output voltage—in other words, the zero at the origin is cancelled by a new pole at the origin. At low frequencies, the remaining pole at $s = -1/RC$ has minimal effect. As the signal frequency increases, first order low-pass behavior will be observed.

Once the output is integrated, the differential capacitance $C_{p2} - C_{p1}$ must be determined in order to identify the sensor gain and recover the original input signal. If this capacitance is not known, the output will include an unknown constant scaling factor.

III. Analog implementation

There are two factors which determine the sensitivity and performance of the sensor: the geometry of the sensor plates, and the quality of the differential amplifier that is attached to them. Since the sensor should measure the voltage on one nearby wire without mixing in voltages from more distant wires, the sensor plates should not be made too large. The capacitance of the sensor plates then determines the maximum admissible input bias currents for the differential amplifier.

Based on the size of service entry cable and typical clearance constraints around existing wiring, the sensor plates are designed to have an area of $1\,\mathrm{cm}^2$. To minimize the cost of fabrication, the plates are built into the bottom two layers of a standard $1.6\,\mathrm{mm}$ four-layer printed circuit board (PCB). In a standard FR4 PCB, the bottom two layers are separated by $0.25\,\mathrm{mm}$ of laminate with a

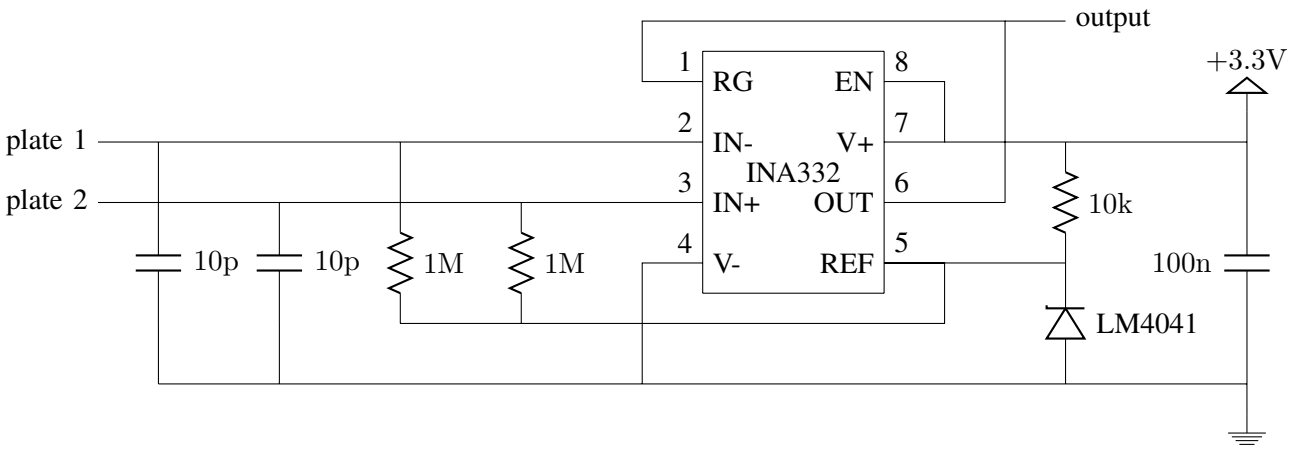

Fig. 2. Sensor circuit using a TI INA332 instrumentation amplifier and a TI LM4041 voltage reference. The combined cost of these parts is less than $3 in quantity 1.

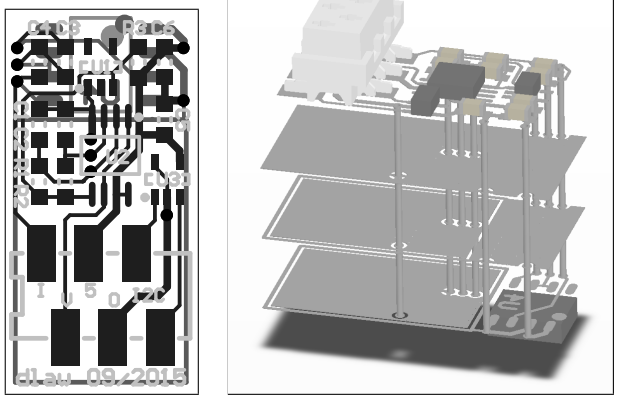

Fig. 3. 2D and 3D exploded views of the sensor PCB. The board dimensions are 1 cm by 2 cm. From top to bottom, layers contain: (1) connector, instrumentation amplifier, and supporting components, (2) ground plane, (3) sensor plate and ground plane, (4) sensor plate and Hall effect IC.

dielectric constant of approximately 4.5. Therefore the inter-plate capacitance is

$$C_{ip} = 4.5 \cdot \varepsilon_0 \cdot \frac{1\,\mathrm{cm}^2}{0.25\,\mathrm{mm}} = 15.9\,\mathrm{pF}.$$

With this information, the differential capacitance between the sensor plates and a nearby wire can be estimated. Suppose that the effective area of overlap between a wire and the sensor plates is $0.5\,\mathrm{cm}^2$, and the wire and the closer plate are separated by $1\,\mathrm{mm}$ of insulation with a dielectric constant of 2.1 (such as Teflon). The capacitance between the wire and the closer plate is

$$C_{p2} = 2.1 \cdot \varepsilon_0 \cdot 0.5\,\mathrm{cm}^2 \cdot 1\,\mathrm{mm} = 0.930\,\mathrm{pF}.$$

Then C_{p1} is given by the series combination of C_{p2} and C_{ip}, i.e.

$$\frac{1}{C_{p1}} = \frac{1}{C_{p2}} + \frac{1}{C_{ip}}$$

and the differential capacitance is

$$C_{p2} - C_{p1} = \frac{C_{p2}^2}{C_{ip} + C_{p2}} = 0.051\,\mathrm{pF}.$$

The amplifier's input bias currents must be much smaller than the currents injected into the bias resistors by C_{p1} and C_{p2}. (This requirement is independent of the resistor values.) The limiting case is the lowest voltage of interest at the lowest frequency of interest—for design purposes, a $1\,\mathrm{V}$ signal at $60\,\mathrm{Hz}$. The differential current produced by this signal is

$$2\pi f(C_{p2} - C_{p1})V = 2\pi \cdot 60\,\mathrm{Hz} \cdot 0.051\,\mathrm{pF} \cdot 1\,\mathrm{V} = 19\,\mathrm{pA}.$$

To avoid distorting the signal, the amplifier's input bias currents should not exceed about $1\,\mathrm{pA}$. A low-cost instrumentation amplifier, such as the Texas Instruments INA332, meets this specification.

In the differential mode, the inter-plate capacitance of C_{ip} is equivalent to a capacitance between each plate and ground of

$$2C_{ip} = 31.8\,\mathrm{pF}.$$

This capacitance reduces the bandwidth of the sensor and should be kept as small as possible. However, the amplifier is susceptible to common-mode disturbances which cause its inputs to exceed their allowable voltage range. In order to have some capacitive filtering of common mode inputs, an additional capacitance of $10\,\mathrm{pF}$ is provided between each sensor plate and ground. This gives a total differential mode plate-to-ground capacitance of

$$C = 41.8\,\mathrm{pF}.$$

The last design task is to select the bias resistors attached to the sensor plates. The sensor gain is given by sRC_d, so to maximize sensitivity R should be as large as possible. However, larger values of R increase the time constant RC and decrease the sensor bandwidth. A good balance between these requirements is achieved by $R = 1\,\mathrm{M}\Omega$. The breakpoint of the input network is placed at

$$\frac{1}{2\pi RC} = 3.81\,\mathrm{kHz}$$

which is significantly faster than the signals of interest, but the sensor gain remains large enough to obtain usable voltage signals out of the amplifier.

Using (5), the transfer function of the specified analog sensor is

$$\frac{V_o(s)}{V_i(s)} \approx \frac{s \cdot 51\,\mathrm{ns}}{s \cdot 42\,\mu\mathrm{s} + 1}. \tag{6}$$

For sufficiently low frequencies, (4) applies and

$$\frac{V_o(s)}{V_i(s)} \approx s \cdot 51\,\mathrm{ns}.$$

The final analog sensor schematic is given in Fig. 2 and the PCB is depicted in Fig. 3. Because of the high impedances present on the PCB, special care must be taken to include guard traces around sensitive nodes and to clean conductive residue from the board after assembly. (Because the new voltage sensor is intended for non-contact power metering applications, this PCB also includes footprints for a Hall effect-based magnetic field sensor, an EEPROM, and a connector for cabled attachment to a microcontroller.)

IV. Digital signal processing

The sensor output must be integrated to recover the original voltage being measured. Past implementations have used an analog integrating filter [8], but better performance is possible by performing the integration digitally. The design of the integrating filter presents a fundamental tradeoff between accuracy and disturbance rejection. Specifically, there are three design requirements:

1) The filter must faithfully reconstruct the voltage being measured.
2) The filter must reject low frequency disturbances, such as those caused by thermal drift.
3) The filter must recover quickly from impulsive disturbances.

These requirements correspond to the following three properties of a linear filter:

1) The filter's frequency response should be inversely proportional to the frequency, and introduce 90 degrees of phase lag, for every frequency present in the voltage being measured.
2) The filter's frequency response should roll off quickly below the frequencies of interest.
3) The filter's impulse response should be short.

These goals have previously been realized by a cascade of two analog filters: a high-pass filter which admits the signals of interest but blocks low frequency disturbances, followed by an integrator to recover the original voltage signal. The challenge is that a causal analog filter cannot have a sharp transition between its stop band and pass band without introducing significant phase distortion—but if the transition to the stop band is gradual, low frequency disturbances will be admitted and amplified by the integrator.

Throughout this section, ω refers to a normalized angular frequency with units of radians per sample. Suppose that there are $2N$ samples per line cycle, so that the frequency of the nth harmonic is $\pi n/N$ radians per sample. The frequency response of an ideal integrating filter is given by

$$H_i(\omega) = \frac{\pi}{j\omega N}. \tag{7}$$

(This filter is "ideal" only in that it integrates signals perfectly and has a unit magnitude response at line frequency. It does not satisfy the second and third filter requirements.)

If the sampled line frequency of π/N radians per sample corresponds to $60\,\mathrm{Hz}$ in continuous time, the frequency response of the analog filter in [8] is given by

$$H_a(\omega) = \frac{j\omega\pi/N}{(j\omega + 1/\tau_0)(j\omega + 1/\tau_1)} \tag{8}$$

with

$$\tau_0 = (2.2\,\mu\mathrm{F}) \cdot (12.1\,\mathrm{k}\Omega) \cdot (60\,\mathrm{Hz}) \cdot 2N$$
$$\tau_1 = (2.2\,\mu\mathrm{F}) \cdot (47\,\mathrm{k}\Omega) \cdot (60\,\mathrm{Hz}) \cdot 2N.$$

This analog filter is compared with two digital finite impulse response (FIR) filters. The FIR filters have antisymmetric impulse responses (such filters are known as "Type 3" FIR filters). As a consequence, they have zero group delay, introduce 90 degrees of phase lag at all frequencies, and do not pass signals at zero frequency or at the Nyquist rate.

The first FIR filter is the Type 3 filter with $2N - 1$ taps whose frequency response H_1 satisfies

$$H_1\left(\frac{\pi n}{N}\right) = \frac{1}{jn} \qquad n \in \mathbb{Z},\ 1 \le |n| < N.$$

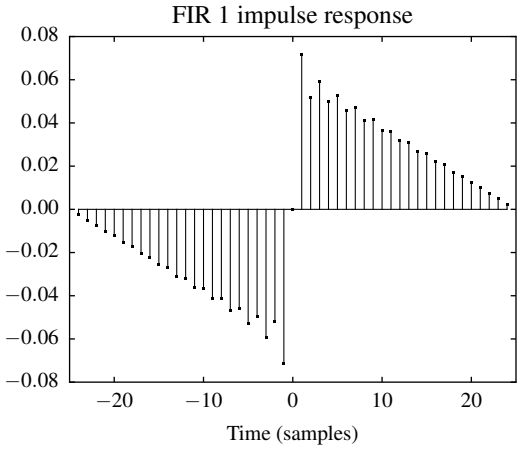

Fig. 4. Impulse response $h_1[t]$ for $N = 25$. The impulse response is zero when $|t| \geq 25$.

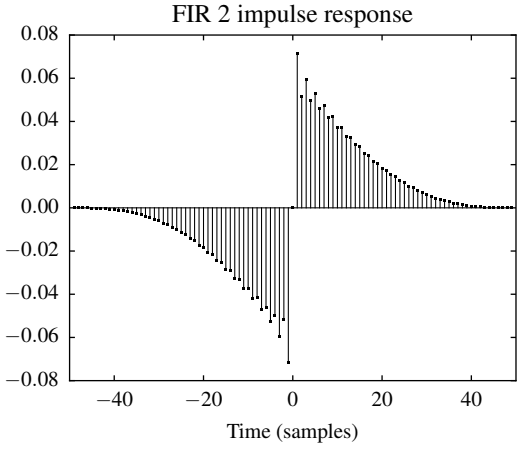

Fig. 5. Impulse response $h_2[t]$ for $N = 25$. The impulse response is zero when $|t| \geq 50$.

The second FIR filter is the Type 3 filter with $4N - 1$ taps whose frequency response H_2 satisfies

$$H_2\left(\frac{\pi n}{2N}\right) = \frac{2c_n}{jn} \qquad n \in \mathbb{Z},\ 1 \leq |n| < 2N$$

with

$$c_n = \begin{cases} 1/2 & |n| = 1 \\ 1 & 2 \leq |n| < 2N - 1 \\ 3/4 & |n| = 2N - 1. \end{cases}$$

The filter impulse responses are computed using the inverse discrete Fourier transform:

$$h_1[t] = \frac{1}{N} \sum_{n=1}^{N-1} \left(\frac{1}{n} \cdot \sin\left(\frac{\pi n t}{N}\right)\right) \qquad |t| < N \quad (9)$$

$$h_2[t] = \frac{1}{N} \sum_{n=1}^{2N-1} \left(\frac{c_n}{n} \cdot \sin\left(\frac{\pi n t}{N}\right)\right) \quad |t| < 2N \quad (10)$$

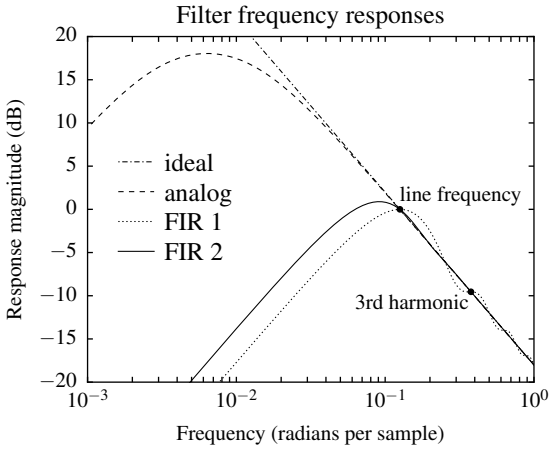

Fig. 6. Magnitude behavior of the filters for $N = 25$. Note the logarithmic horizontal scale. The analog filter introduces phase distortion which is not depicted on this plot. Amplification of low frequency disturbances is roughly proportional to the area under the left half of the response curve.

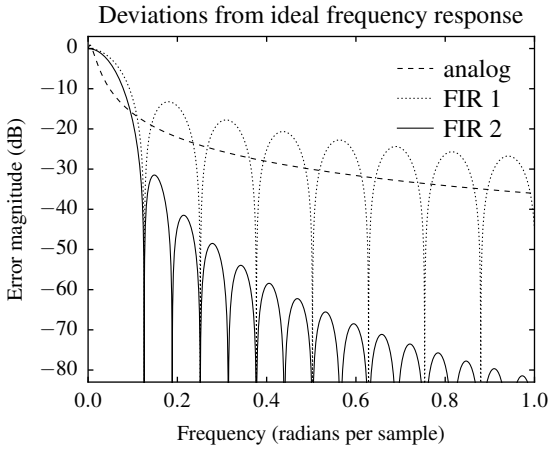

Fig. 7. Magnitudes of the relative deviations from the ideal frequency response for $N = 25$. Both of the FIR filters have zero error at line frequency and its harmonics. Deviation from the ideal response is necessary and desirable at frequencies below line frequency.

where t is an integer representing the discrete time. The impulse responses are plotted in Fig. 4 and Fig. 5.

By definition, $H_1(\omega) = H_2(\omega) = H_i(\omega)$ at line frequency and all of its harmonics below the Nyquist rate. h_1 is the shortest impulse response whose Fourier transform has this property, and h_2 is designed to have a smoother frequency response at the expense of being twice as long as h_1.

From the impulse responses, the discrete time Fourier transform gives the continuous frequency responses. The analytical expressions are omitted here because they provide no additional insight. Fig. 6 shows the magnitude response of each filter and Fig. 7 shows the relative mag-

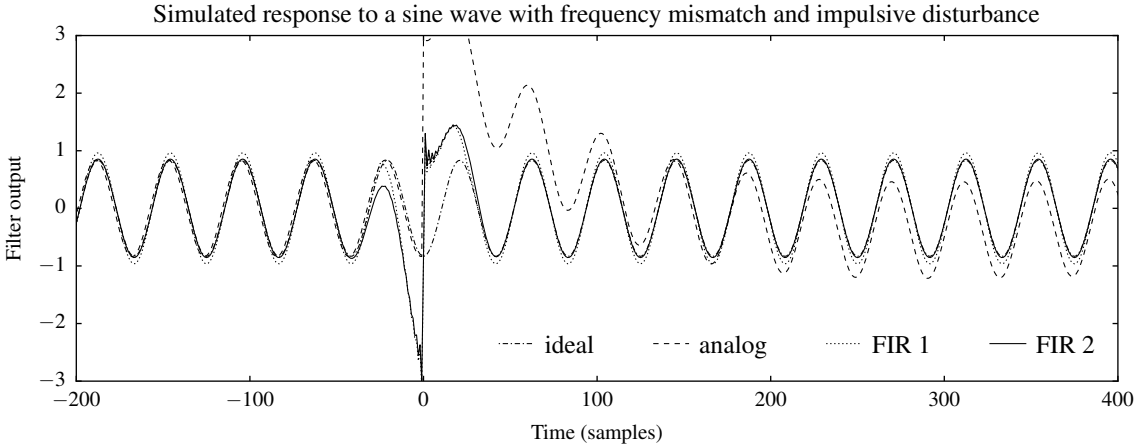

Fig. 8. Simulated response of the filters to an impulsive disturbance with magnitude 30 at $t = 0$. The disturbance affects FIR 1 for $-25 < t < 25$ and FIR 2 for $-50 < t < 50$, but the analog filter has not yet recovered from the disturbance at $t = 400$. The filters are designed for a line frequency of $50\,\mathrm{Hz}$ with $N = 25$, but the input signal is provided at $60\,\mathrm{Hz}$ to demonstrate that the filters perform well even when line frequency is not known in advance.

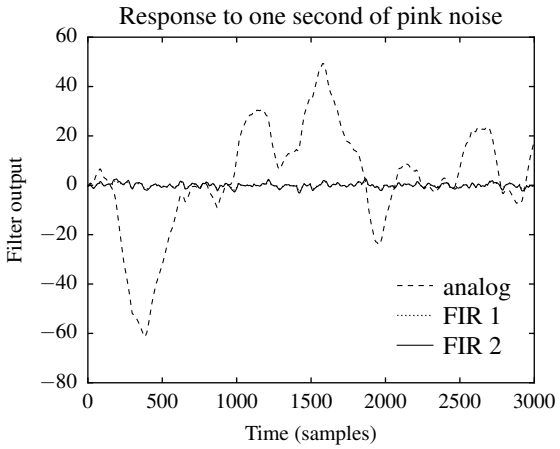

Fig. 9. Simulated response of each filter to the same sequence of pink noise. The pink noise was generated as the cumulative sum of a sequence of numbers chosen uniformly at random between -0.5 and 0.5.

nitude of the difference between each filter's response and the ideal response.[2]

We consider the response of each filter to the signal

$$x[t] = \sin(\pi t/N \cdot 60/50) + 30\delta[t].$$

This represents the case where the digital filters were designed for a line frequency of $50\,\mathrm{Hz}$ but the actual frequency is $60\,\mathrm{Hz}$, and an impulsive disturbance of magnitude 30 occurs at time $t = 0$.[3] These responses are plotted in Fig. 8 and exemplify the benefits and drawbacks of each type of filter.

Lastly, to illustrate the superior disturbance rejection of the digital filters, the output of each filter is computed for the same input sequence of pink (i.e. $1/f$) noise. The results are plotted in Fig. 9. Clearly, the analog filter exhibits a greater amount of error amplification.

Although the FIR filters are non-causal, both become causal when composed with a finite time delay. It is therefore possible to implement them, with the caveat that the output will not be known in real time. In particular, the first FIR filter delays its outputs by half of a line cycle and the second FIR filter delays its outputs by one full line cycle.

V. Experimental results

The new voltage sensor was used together with Hall effect magnetic field sensors to perform non-contact power metering as described in [8] and shown in Fig. 10. The non-contact power meter was installed in parallel with a traditional power meter so that the results could be compared. Various electrical loads were switched on and off in order to obtain the time series data depicted in Fig. 11. Mismatch between the traditional power meter and the non-contact power meter did not exceed $10\,\mathrm{W}$ over a dynamic range of $1000\,\mathrm{W}$, showing that the new

[2]For a frequency response $H(\omega)$, the exact function plotted in Fig. 6 is $20\log_{10}|H(\omega)|$ and the exact function plotted in Fig. 7 is $20\log_{10}|H(\omega)/H_i(\omega) - 1|$.

[3]Such disturbances often occur when a large inductive load is disconnected, resulting in a high instantaneous rate of voltage change on the inductor. This produces a powerful electric field which causes the sensor plate voltages to briefly exceed the common-mode input range of the amplifier. The INA332 drives its output to the positive rail when this condition occurs.

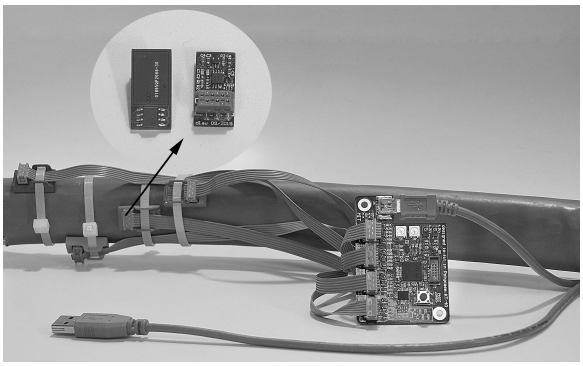

Fig. 10. Non-contact power meter using the new voltage sensors installed on a service entrance cable for power metering.

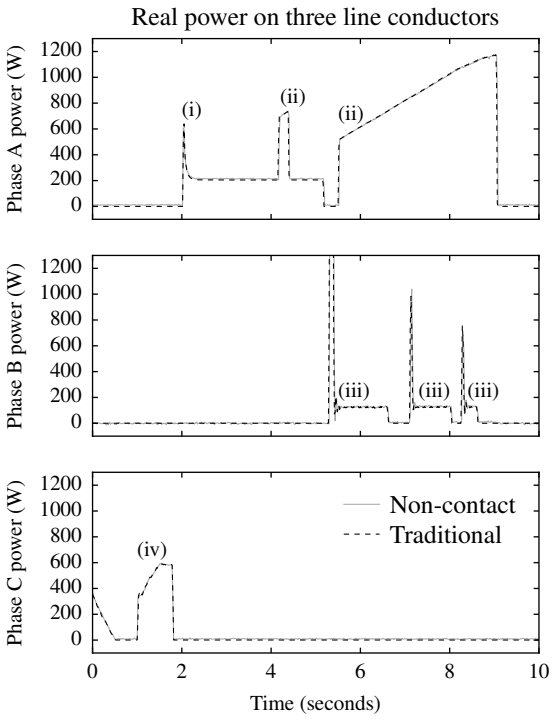

Fig. 11. Data collected by non-contact and traditional power meters. The turn-on transients depicted are from (i) a 250 W incandescent lightbulb, (ii) a 1500 W space heater, (iii) an 0.25 hp induction motor, and (iv) a 600 W bank of dimmable incandescent lightbulbs.

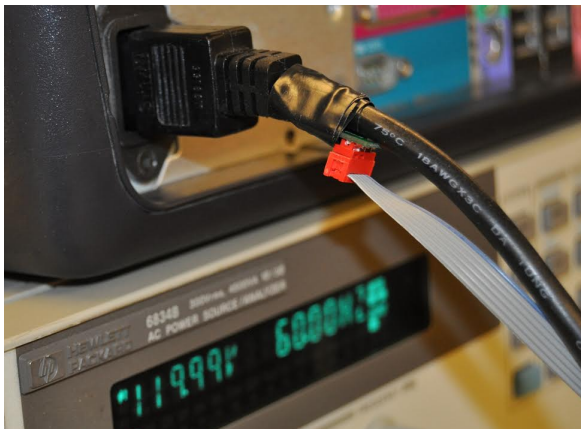

Fig. 12. Non-contact voltage sensor attached to an 18-AWG computer power cable powered by an HP 6834B AC source. The ribbon cable leads to a printed circuit board which implements the analog filter and two digital FIR filters.

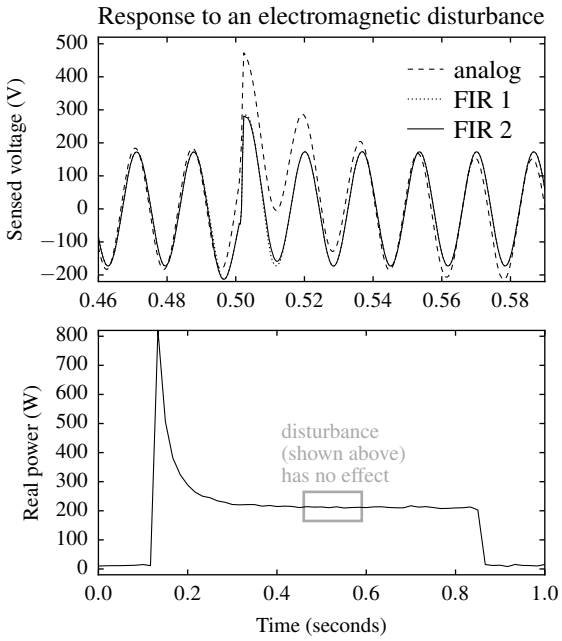

Fig. 13. Response of the voltage sensor to a 100 mA fan motor being turned off 30 cm away from the sensor at $t \approx 0.5$. The digital filter recovers from the electromagnetic disturbance quickly, so *non-contact power metering is not affected by the disturbance*.

voltage sensor was able to accurately distinguish real and reactive power.

In order to obtain more detailed results showing the performance of the new digital filters, the voltage sensor was attached to an 18-AWG computer power cable with line voltage supplied by an HP 6834B AC source. (This cable was chosen because thinner conductors produce the smallest coupling capacitance and therefore pose the most difficult sensing challenge.) This experimental setup is shown in Fig. 12. The sensor was attached to an Atmel SAM4S microcontroller, which sampled the sensor with its built in ADC at a sample rate of 3 kHz and processed the signal using both of the FIR filters. The analog filter of [8] was constructed using a Texas Instruments OPA4376 operational amplifier and its output was connected to a second ADC channel. The output from all three filters was streamed from the microcontroller to a computer. With a line frequency of 60 Hz, there were 50 samples per line cycle and $N = 25$.

The output voltage from each filter was measured for sinusoidal inputs at various voltages and frequencies.

Input V RMS	Analog % error	FIR 1 % error	FIR 2 % error	Analog phase error, degrees
30	5.7	2.3	2.3	8.92
60	3.7	1.6	1.6	9.04
90	1.1	0.0	0.0	9.07
120	0.3	0.0	0.0	9.09
150	1.0	1.2	1.2	9.11
180	−0.5	0.8	0.8	9.16
210	−2.2	−0.0	−0.0	9.21
240	−3.3	−0.1	−0.1	9.29
270	−3.8	0.3	0.3	9.34
300	−4.5	0.5	0.5	9.40

TABLE I
OUTPUT ERROR FROM EACH FILTER FOR VARIOUS INPUT VOLTAGES AT 60 Hz.

Input Hz	Analog % error	FIR 1 % error	FIR 2 % error	Analog phase error, degrees
60	5.7	2.3	2.3	8.92
120	2.9	−1.7	−1.7	4.98
180	2.5	−2.7	−2.7	3.69
240	1.9	−3.8	−3.8	3.06
300	1.6	−4.2	−4.2	2.69
360	0.8	−5.2	−5.2	2.48
420	0.1	−6.2	−6.2	2.33
480	−1.3	−7.6	−7.6	2.22
540	−2.8	−9.1	−9.1	2.16
600	−4.8	−11.2	−11.2	2.14

TABLE II
OUTPUT ERROR FROM EACH FILTER FOR VARIOUS INPUT FREQUENCIES AT 30 V RMS.

Equation (4) was solved to find that the differential capacitance was 1.22 pF at 120 V and 60 Hz. At other voltages and frequencies, the percent magnitude error was computed for the output of each filter. The phase error of the analog filter relative to the (zero-phase) digital filters was also computed. This data is given in tables I and II.

The collected data shows that the digital filters significantly outperform the analog filter with respect to phase lag and voltage linearity. As predicted by (5), all filters suffer from frequency-dependent gain, with a slightly more pronounced effect for the digital filters.[4] The new sensors with digital filters exhibit error less than 5% over all voltages up to 300 V and frequencies up to 300 Hz.

Finally, the disturbance rejection of each filter was tested by turning off a 100 mA fan motor at a distance of 30 cm away from the sensor. (The motor does not have a clamp circuit, so an inductive voltage spike generates a strong electric field every time it is turned off.) The response of the three filters to this situation is shown in Fig. 13. There is good agreement with the simulated behavior in Fig. 8. The digital filters are only affected by the disturbance for one or two line cycles, but the analog filter has not recovered after many line cycles. Fig. 13 also shows that the digital filters prevent the disturbance from affecting power metering.

[4]If the additional frequency-dependent attenuation is carefully measured, the frequency response H_2 may be shaped to eliminate the frequency dependence at no additional computational cost by slightly altering the coefficients c_n used in its construction.

VI. CONCLUSIONS

Non-contact sensors allow the measurement of high voltages in a constrained setting without the need for high-voltage isolation or a complex installation. Careful design of a digital filter improves the accuracy and disturbance rejection of the capacitively coupled voltage sensor. With the new digital filters, linearity is better than ±5% up to 300 V and 300 Hz.

Microcontrollers with integrated ADCs are sufficiently inexpensive that even with the digital filter and all supporting hardware, the new voltage sensor can be built for less than $10 of parts. If exact measurement of voltage is needed, the new sensor must be calibrated against a known reference voltage. But many power quality metrics—such as total harmonic distortion and line regulation—are unaffected by changes of a constant scaling factor.

The new sensor's superior accuracy and disturbance rejection enable non-contact power metering to succeed in spite of electromagnetic disturbances. Together with the sensor's low cost, this makes the use of non-contact voltage sensors practical in a wide variety of new applications.

REFERENCES

[1] W. A. Zisman, "A new method of measuring contact potential differences in metals," *Review of Scientific Instruments*, vol. 3, pp. 367–370, Mar. 1932.

[2] W. E. Vosteen, "A high speed electrostatic voltmeter technique," in *Industry Applications Society Annual Meeting*, Oct. 1988, pp. 1617–1619.

[3] D. Grant, G. Hearn, W. Maggs, and I. Gonzalez, "An electrostatic charge meter using a microcontroller offers advanced features and easier atex certification," *Journal of Electrostatics*, vol. 67, pp. 473–476, May 2009.

[4] L. Wu, P. Wouters, E. van Heesch, and E. Steennis, "On-site voltage measurement with capacitive sensors on high voltage systems," in *IEEE Trondheim PowerTech*, Jun. 2011, pp. 1–6.

[5] J. Bobowski, S. Ferdous, and T. Johnson, "Calibrated single-contact voltage sensor for high-voltage monitoring applications," *IEEE Trans. Instrum. Meas.*, vol. 64, pp. 923–934, Apr. 2015.

[6] K. M. Tsang and W. L. Chan, "Dual capacitive sensors for non-contact ac voltage measurement," *Sensors and Acturators A: Physical*, vol. 167, pp. 261–266, Jun. 2011.

[7] D. Balsamo, D. Porcarelli, L. Benini, and B. Davide, "A new non-invasive voltage measurement method for wireless analysis of electrical parameters and power quality," in *IEEE Sensors*, Nov. 2013, pp. 1–4.

[8] J. S. Donnal and S. B. Leeb, "Noncontact power meter," *IEEE Sensors J.*, vol. 15, pp. 1161–1169, Feb. 2015.